Schmidt-hammer exposure-age dating of talus slopes in upper Jostedalen, southern Norway: Interpreting the age and development of diachronous surfaces

John A Matthews[1] [iD] and Richard W. Mourne[2]

Abstract

Schmidt-hammer exposure-age dating (SHD) was used to evaluate the surface age, dynamics and evolution of eight talus (scree) slopes located between ~520 and ~1010 m a.s.l. in the upper Jostedalen area of southern Norway. Statistically significant differences in mean *R*-values were found between talus slopes but there was no consistent difference in *R*-values between three mid- to lower-slope positions, two operators, or first and second impacts from the same boulders. A new regional age-calibration equation yielded SHD ages ranging from 8425 ± 700 years to 2620 ± 740 years. SHD ages from talus slopes and other landforms with diachronous surfaces (such as alluvial fans, snow-avalanche fans, pronival ramparts and rock glaciers) represent the average exposure age of the surface boulders and provide insights into landform evolution. Here, our SHD ages are interpreted in terms of Early Holocene paraglacial rock-slope instability, Mid-Holocene permafrost degradation, low but possibly variable rates of rockfall activity in the Late-Holocene, and spatial variations affected by local site differences. Survival of rock particles with relatively old exposure ages towards the distal margins of the talus slopes is attributed to their slow development with low levels of modern activity. SHD ages from diachronous surfaces may considerably underestimate landform age (defined as the onset of landform formation). Greater application can be anticipated, however, in the inference of landform dynamics from the *R*-value distributions of diachronous surfaces and in the use of SHD age as an indicator of the extent of modern activity.

Introduction

Talus (scree) slopes are well-known periglacial landforms that are typically formed by the accumulation of rockfall debris (talus) downslope of bedrock cliffs subject to frost weathering. The standard model of rockfall talus slope form and development envisages a rectilinear upper (proximal) slope segment with a surface gradient of ~33°–38°, and a lower (distal) slope segment that is concave in profile (Ballantyne, 2018; Luckman, 2013; Francou and Manté, 1990; Rixhon and Desmoulin, 2013; Sanders, 2010; Statham, 1976). The surface layer of the talus slope often consists exclusively of boulders, which tend to exhibit a downslope increase in size due to fall sorting whereby larger clasts have greater momentum and travel farther. However, as talus accumulates, the upper slope segment increases in height and extends at the expense of the lower slope segment while cliff height diminishes. Relatively few boulders would then have sufficient kinetic energy to travel the increased distance necessary to reach the distal segment. On mature talus slopes, therefore, boulders on the surface of the distal segment may fail to be buried by later rockfall material and hence may survive in the landscape as relicts and exhibit greater exposure ages. Preservation potential is enhanced by the high volume of voids between the boulders leading to free drainage, a lack of surface water and a sparse vegetation and soil cover.

Previous dating of talus has been attempted based on various techniques, including weathering-rind thickness (Chinn, 1981; Whitehouse and McSaveney, 1983; Whitehouse et al., 1980), lichenometry (McCarroll, 1994; McCarroll et al., 1998, 2001; Sass, 2010), dendrochronology (Lafortune et al., 1997; Moya et al., 2010; Perret et al., 2006; Šilhán, 2010; Stoffel et al., 2006) and radiocarbon dating using buried palaeosol material (Blikra and Nemec, 1998; Curry and Black, 2003; Hétu and Gray, 2000; Hinchliffe and Ballantyne, 2009; Innes, 1983). Several previous studies have included SHD of talus samples (e.g. Nesje et al., 2021; Peña-Monné et al., 2024; Santos-González et al., 2024; Scapozza et al., 2021; Scotti et al., 2017; Sumner et al., 2002) but talus was not the focus of these studies and detailed dating of talus using SHD methods has not been attempted.

[1]Department of Geography, Swansea University, UK
[2]School of Architecture and Environment, University of the West of England, UK

Corresponding author:
John A Matthews, Department of Geography, Swansea University, Singleton Park, Swansea Wales SA2 8PP, UK.
Email: J.A.Matthews@Swansea.ac.uk

Schmidt-hammer exposure-age dating (SHD) is used for calibrated-age dating of weathered bedrock surfaces and the boulder surfaces associated with depositional landforms (see the comprehensive review of Matthews and Winkler, 2022). SHD provides a relatively simple, non-destructive and inexpensive method that has been found particularly useful in glacial and periglacial landscapes where exposed bedrock and boulder surfaces are extensive, the organic material needed for several alternative dating techniques (such as radiocarbon dating, lichenometry and dendrochronology) is sparse and there are relatively few restrictions on obtaining the necessary large number of Schmidt-hammer measurements. In Scandinavia, the technique has been applied over the last decade to a wide range of active and relict periglacial landforms, including rock glaciers, pronival ramparts, snow-avalanche landforms, patterned ground, block streams, rock-slope failures, alluvial fans and cryoplanation terraces (see Matthews and Nesje, 2022 and references therein).

SHD is underpinned by the principle that the hardness and compressive strength of a rock surface declines following exposure to subaerial weathering and hence is time dependent (Matthews and Winkler, 2022). Schmidt hammers measure *R*-values, that is the 'rebound values' or 'rebound numbers', of a spring-loaded plunger as it impacts a rock surface. The decline in *R*-values with time since exposure to the atmosphere proceeds at a rate that is determined by age-calibration (i.e. defining the numerical relationship between *R*-value and rock-surface age for surfaces of known age). Based on large samples of *R*-values, the age-calibration equation is used to predict the exposure age of similar rock surfaces of unknown age within statistical confidence intervals.

Although talus slopes provide landscape surfaces that may appear suitable for the application of SHD, they present the technique with a number of challenges that are not experienced by synchronous surfaces (i.e. surfaces built in one event and then abandoned and hence entirely composed of material with the same exposure age, such as recessional moraines and rock-slope failures). As well as the burial of surface material during talus-slope development, the surface material of an active talus slope is typically unstable and, during the accumulation of talus, previously deposited debris is commonly reworked (Hinchliffe, 1999; Stoffel et al., 2006). Furthermore, variations in the quantity of rock fall and hence the talus accumulation rate may occur due to changes in the environment, including the intensity of the paraglacial response of slopes to deglaciation (André, 1997; Hinchliffe, 1999; Hinchliffe and Ballantyne, 2009) and climatic changes during the Holocene (Hétu and Gray, 2000; Innes, 1983; Stoffel et al., 2005a, 2005b). Like many other landform surfaces, including, for example, the surfaces of alluvial fans, pronival ramparts and rock glaciers, the surface of the talus slope tends therefore to be diachronous (i.e. constructed continually or incrementally and hence composed of a boulder population of mixed exposure ages). The average exposure age of the talus surface may therefore bear little or no relationship to landform age defined as the time elapsed since the onset of talus-slope formation. It can nevertheless provide insights into the timing of rock-fall activity and the development of talus slopes in relation to environmental change, including climatic change. Thus, SHD of talus is of interest not only for broadening the range of applications of this dating technique and for improving our understanding of the dynamics and evolution of talus slopes but also for potential insights into the application of SHD to other landforms characterised by diachronous surfaces.

The four main aims of this paper can therefore be summarised as follows: (1) to present the first detailed application of SHD to talus slopes; (2) to determine the exposure ages of the boulder surface of several talus slopes in the upper Jostedalen region of southern Norway; (3) to evaluate the potential of SHD for determining talus-slope age, dynamics and evolution; and (4) to
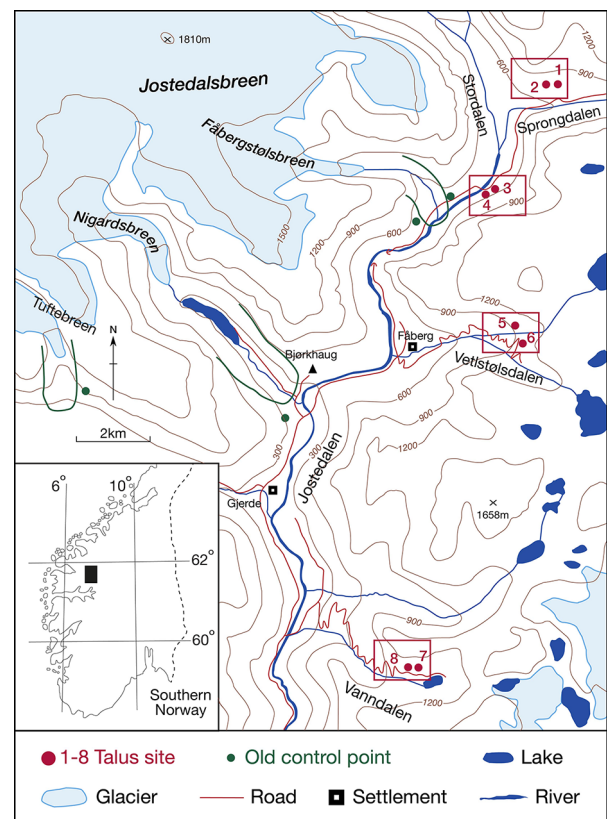
Figure 1. Location of eight talus sites (numbered) in Sprongdalen, Stordalen, Vetlestølsdalen and Vanndalen, upper Jostedalen region, southern Norway. The location of Bjørkhaug meteorological station (Δ) at 324 m a.s.l. and old control points outside the Little Ice Age glacier forelands of three Jostedalsbreen outlet glaciers are also shown. Glacier-foreland boundaries (green lines) are defined in the field by latero-terminal moraines. Rectangles (red) identify the areas covered in Figures 2 and 3.

consider the usefulness of SHD more broadly in the context of diachronous surfaces.

Study area

Talus slopes are located downslope of bedrock cliffs in several valleys east of the Jostedalsbreen ice cap in the upper Jostedalen area of southern Norway (Figure 1). We selected the eight longest talus slopes in Stordalen and the tributary valleys of Sprongdalen, Vetlestølsdalen and Vanndalen, where the talus is typically dominated by coarse, boulder-sized debris (Figures 2–4). Sites in the former two valleys lie in the sub-alpine zone but are not tree covered due to the coarse substrate, whereas the latter two valleys are located above the tree line in the alpine zone. Site altitudes (distal talus surfaces) range from ~520 m to ~1010 m a.s.l. with south- or west-facing aspects.

Based on climatic normals (AD 1961–1990) from Bjørkhaug weather station located on Figure 1 at 324 m a.s.l. (adjusted for a temperature gradient of −0.6°C per 100 m rise in altitude), estimated mean annual air temperature (MAAT) at the sites is between −2.5°C and −0.5°C (Aune, 1993). Corresponding mean July and January air temperatures are 9.2°C–12.2°C and −0.5°C to 2.5°C, respectively. Mean annual precipitation totals are ~1400 mm (Førland, 1993), and snow depths are up to ~4.0 m (http://www.senorge.no). Bedrock is predominantly granite and granitic gneiss (Lutro and Tveten, 1996) and this is reflected in the talus boulders.

All sites are located well beyond the prominent 'Little Ice Age' moraines that extend up to 5 km from the present day limits
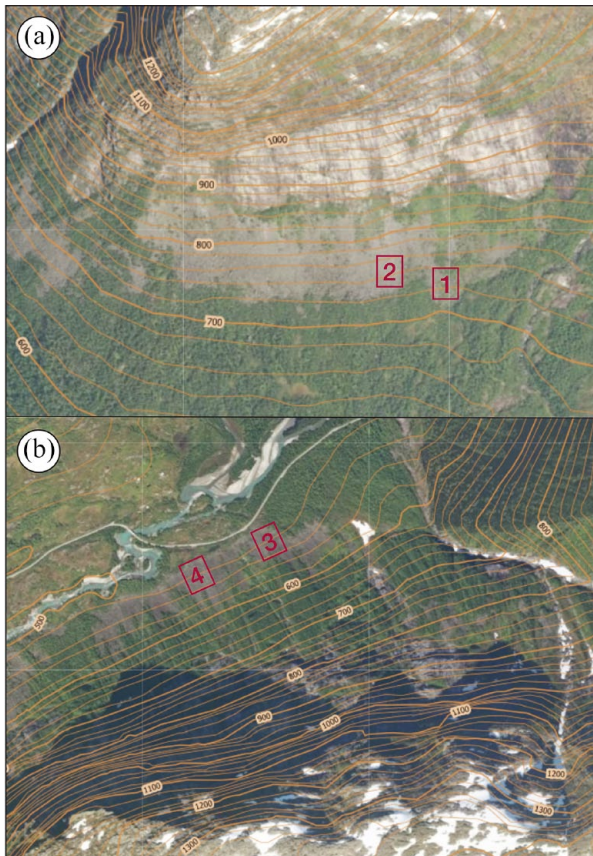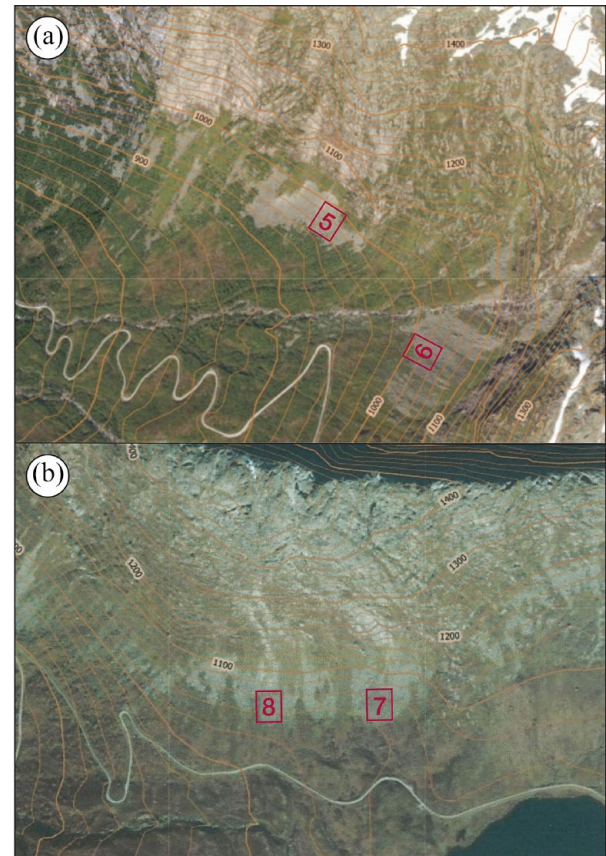
Figure 2. Landscape setting of the talus sites in Sprongdalen (a, Sites 1 and 2) and Stordalen (b, Sites 3 and 4) from aerial photographs with superimposed contours at 100 m intervals (http://www.norgeibilder). Sites are 60 m × 40 m as shown in Figure 4.

Figure 3. Landscape setting of the talus sites in Vetlestølsdalen (a, Sites 5 and 6) and Vanndalen (b, Sites 7 and 8) from aerial photographs with superimposed contours (http://www.norgeibilder). Sites are 60 m × 40 m as shown in Figure 4.

of the main outlet glaciers of the Jostedalsbreen ice cap. The maximum extent of the glaciers in the Little Ice Age has been precisely dated to the mid-eighteenth century by historical evidence (e.g. Gjerde et al., 2023; Grove, 1988; Østrem et al., 1977). Early-Holocene moraines located up to about 1 km beyond these Little Ice Age limits have been dated by radiocarbon and ^{10}Be to the Erdalen Event at 10,200–9,700 cal years BP (Dahl et al., 2002; Matthews et al., 2008). Prior to the Erdalen Event, Jostedalen and its neighbouring valleys were deglaciated by ~10,200 cal years BP following the very rapid temperature rise that occurred at the transition from Younger Dryas to Holocene (Eldevik et al., 2014; Mottershead and Colin, 1976; Nesje, 2009; Nesje and Matthews, 2024; Nesje et al., 1991). With the possible exception of nunataks, the whole region was ice-covered during the Younger Dryas (Hughes et al., 2016; Mangerud et al., 2023; Matthews et al., 2023)

Methods

R-value measurements were made using two original mechanical *N*-type Schmidt hammers (Proceq, 2017). Care was taken to reduce possible sources of non-age-related variability (Matthews and Winkler, 2022). Use only of boulders composed of granite or granitic gneiss ensured that the effects of lithological differences were minimised (cf. Matthews et al., 2016; Tomkins et al., 2016, 2018a). All measurements were made in dry conditions (Karakul, 2017; Sumner and Nel, 2002). Impacts were restricted to horizontal or near-horizontal surfaces where possible (cf. Karakul, 2020). Rock-surface irregularities, cracks, joints, edges and flakes, and lichen and moss cover were avoided (Matthews and Owen, 2010; Shakesby et al., 2006). Rock-surface smoothing using a

carborundrum stone was not attempted (cf. Shepherd et al., 2024). Other possible rock-surface pretreatment (cleaning) of the rock surfaces was not attempted other than removal of moss and loose rock particles by hand picking.

Outliers (anomalous readings) were not discarded other than those resulting from plunger slippage. Other possible causes of anomalous readings, such as minor surface irregularities, individual minerals or hidden fractures, cannot be identified with certainty. These are assumed to randomly affect *R*-values from both the control surfaces and the surfaces to be dated, and to represent a relatively small component of the large natural variability in *R*-values that affect rock surfaces of the same age.

On each of the eight talus slopes, *R*-values were recorded in a grid of six, 400 m² plots (20 m × 20 m) using the sampling design shown in Figure 5. In each plot, two impacts were made at different spots on 50 of the largest boulders, providing replicate samples of size *n* = 50. The sample of 50 first impacts was designated R_1 and the sample of second impacts was designated R_2. Two operators (O_1 and O_2) sampled adjacent plots at three levels – occupying lower (L_1), mid (L_2) and upper (L_3) slope positions on the distal half of the talus slope. This design allowed variability in mean *R*-values between first and second impacts, between operators and between levels on the talus to be measured and any differences to be tested statistically.

Age-calibration of mean *R*-values employed the 'two-point solution' as developed by Matthews and Owen (2010), Matthews and Winkler (2011) and Matthews and McEwen (2013) and summarised in Matthews and Winkler (2022) using a new linear calibration equation based on young and old surfaces of known age (control points). Although an approach to age-calibration based on two control points has the statistical weakness of being unable
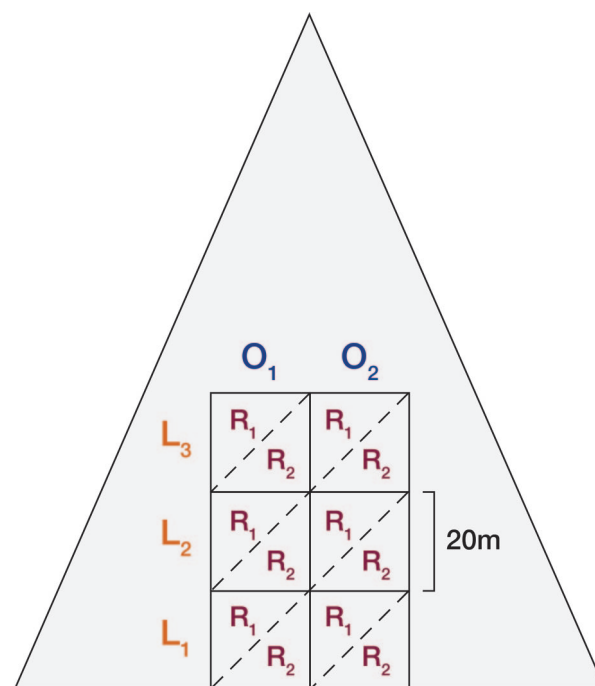
Figure 4. Representative photographs of talus slope characteristics in (a) Stordalen and (b) Vanndalen (note Shogun and person for scale, respectively).

Figure 5. Sampling design on a hypothetical talus cone. Schmidt-hammer R-values were recorded from 50 boulders within each of six plots each measuring $20\,m \times 20\,m$; two impacts per boulder are designated R_1 and R_2. Plots were located in a grid at three levels (L_1–L_3) on the talus slope and adjacent plots were recorded by two operators (O_1 and O_2).

to prove the existence of a linear relationship between mean R-value and exposure-age, it can be justified on empirical and theoretical grounds. Most importantly, in applications where a sufficiently large number control points are available a linear relationship can be demonstrated, at least over the relatively short Holocene timescale (e.g. Shakesby et al., 2011; Tomkins et al., 2018a). Because chemical weathering rates are slow on crystalline rock surfaces, the non-linear weathering rate expected over longer timescales (Colman and Dethier, 1986) and detectable using control-points exposed on 10^4–10^5 timescales (Stahl et al., 2013; Tomkins et al., 2018b) can be rejected. Instead, it can be assumed that the exposure-age/R-value relationship is approximately linear in the present context involving gneissic lithologies over a timescale of ~10 ka. This is fortunate given the *force majeure* of a lack of suitable surfaces intermediate in age between young and old control points in the region.

The two control points actually used in this study are summarised together with other potential control points of similar exposure-age from the region in Table 1. Unweathered talus boulders recognised from their clean rock surfaces without moss or lichen growth provided the young control point mean R-value of 59.67 ± 1.06. This is the mean R-value from 142 boulders on 6 of the 8 talus slopes investigated in Sprongdalen, Vetlestølsdalen and Stordalen. The estimated age of <20 years for these young rock surfaces is based on the time required for the establishment of visible yellow-green lichens (*Rhizocarpon geographicum* agg.) in this area (Bickerton and Matthews, 1992, 1993; Trenbirth and Matthews, 2010).

The other potential young control-point R-values shown in Table 1 are less appropriate on account of the nature of the surface

of unweathered talus boulders, which tends to be rough and irregular. Mean R-values used in previous studies in the area come from glacially-scoured bedrock outcrops (Matthews and Owen, 2010; Matthews et al., 2024) or fluvially transported boulders (Matthews and McEwen, 2013; Matthews et al., 2015), the smoother, abraded surfaces of which yield higher R-values. The mean R-value of 60.67 ± 0.83 obtained from non-abraded bedrock surfaces inside the road tunnel excavated near Fåberg in AD 1979 is in close agreement with and hence supports the validity of the young control-point value used in this study. Rock fracturing during tunnel excavation seems not to have affected the R-values in this case.

Our old control point mean R-value of 38.98 ± 0.97 is the average value obtained from a total of 1800 impacts obtained using identical methods from six glacially scoured granitic bedrock surfaces located outside (distal to) the Little Ice Age glacier forelands of five Jostedalsbreen outlet glaciers (Matthews et al., 2024). Four of these surfaces are associated with the glaciers Fåbergstølsbreen, Nigardsbreen and Tuftebreen (Figure 1). The other two sites are associated with Bødalsbreen and Austerdalsbreen, which are located beyond the area shown in Figure 1. All these old control sites were deglaciated immediately prior to the glacier advance of the Erdalen Event when the outlet glaciers of Jostedalsbreen extended up to 1 km beyond their Little Ice Age extent (Dahl et al., 2002). The use of 10 ka for the age of the old control point in this study is based on radiocarbon dating at Nigardsbreen where Erdalen Event moraines formed at 10,200–9,700 cal. BP (Dahl et al., 2002).

The range of mean R-values between the six outside sites (37.9–40.0 ± 0.97) indicates consistent rates of long-term weathering following exposure for a similar period of time at these sites (discussed fully in Matthews et al., 2024) and hence supports the derivation of a single age-calibration equation for SHD dating of our talus slopes from different valleys in the region. Other potential old control sites included in Table 1 were not used as control

Table 1. Potential control-point *R*-values from granitic lithologies within the broader region (±95% confidence intervals). Young and old control points in bold were used in this study as explained in the text. Values from the other potential control points were not used in this paper but are included in the table for comparative purposes.

Control point	*R*-value mean	No. of impacts	Surface age (year)	Data source
Young control points				
Vetlestølsdalen (boulder berm)	64.42 ± 0.46	625	33	Matthews and McEwen (2013)
4 Jostedalsbreen forelands (bedrock)	65.4–67.9 ± 0.6	300	50–250	Matthews et al. (2024)
Jostedalen road tunnel (bedrock)	60.67 ± 0.83	200	43	This study
6 taluses (unweathered boulders)	**59.67 ± 1.06**	**142**	**<20**	**This study**
Old control points				
Lower Jostedalen (bedrock)	35.34 ± 1.19	1500	~10,000	Matthews and Owen (2010)
6 Jostedalsbreen outside sites (bedrock)	37.9–40.0 ± 1.0	1800	~10,000	Matthews et al. (2024)
6 Jostedalsbreen outside sites (mean)	**38.98 ± 0.97**	**1800**	**~10,000**	Matthews et al. (2024)

points in this study as they yielded less consistent *R*-values, most likely due to small differences in environmental and/or lithological conditions.

The significance of differences between the SHD ages of the talus slopes is judged using 95% confidence intervals (C_t), which combine the statistical errors associated with the calibration equation (C_c) and the sampling error associated with each talus slope (C_s). Variations in the shape of the frequency distributions of *R*-values from each talus slope are used to aid further the interpretation of the SHD ages. This is particularly appropriate for diachronous surfaces, such as talus slopes, where mixed boulder populations of varying age can be expected (Matthews and Winkler, 2022).

Results

Variation in mean R-values

Mean *R*-values derived from first and second impacts combining all the data (*n*=300 impact pairs) from both operators and from all three levels on the eight talus slopes were compared using the non-parametric Wilcoxon matched-pairs signed-ranks test (Matthews, 1981; Siegel, 1956). This tested for a consistent difference between the first and second impacts from the eight talus slopes. The difference in *R*-values from each of the eight talus slopes was very small, ranging from +0.26 (Vanndalen 2) to −1.23 (Vetlestølsdalen 1), and the null hypothesis of no difference between first and second impacts could not be rejected ($p > 0.05$). Application of the same Wilcoxon test of the difference in mean *R*-value between the two operators, which ranged from +2.98 (Sprongdalen 1) to −0.59 (Sprongdalen 2), produced a similar, statistically insignificant result that indicates no consistent operator error.

Small differences in mean *R*-value between the three levels on the eight talus slopes (Table 2) were tested using the non-parametric Friedman two-way analysis of variance by ranks (Matthews, 1981; Siegel, 1956), with the conclusion that there is no consistent difference ($p > 0.05$) between the three levels. Nevertheless, relatively large differences of >4 units between certain levels at two of the taluses (Vanndalen 2 and Sprongdalen 2) are exceptional in that they are statistically significant according to their 95% confidence intervals. In general, however, the non-significant differences in *R*-values between first and second impacts, operators and levels permit similar sample mean values to be combined and relatively large sample sizes to be used for age-calibration and SHD age estimation for each talus slope as a whole (600 impacts).

Calibration equation and predicted SHD ages

The linear calibration equation (y=28,802.34−482.36*x*) derived from the ~20 unit difference between the mean *R*-values of the

two control points of contrasting exposure age is illustrated in Figure 6. Resulting SHD ages for the eight talus slopes, which are summarised in Table 3, can be visualised with reference to Figure 7. All the SHD ages lie between and are significantly different from the exposure ages of the young and old control points. Most exhibit Mid-Holocene ages. SHD ages of 8425 ± 700 (Vanndalen 2) to 2620 ± 740 years (Stordalen 1) demonstrate a wide range of exposure ages from the transition between the Early and Mid-Holocene to the first half of the Late-Holocene.

Non-overlapping confidence intervals in Figure 7 show statistically significant differences in SHD age between many of the talus slopes. In three valleys (Vetlestølsdalen, Sprongdalen and Stordalen), the SHD ages of the two sites do not differ significantly, as indicated by overlapping confidence intervals. Thus, the SHD ages of the talus slopes in Vetlestølsdalen lie between 7.2–4.9 ka with 95% certainty; those in Sprongdalen between 5.0 and 3.5 ka; and those in Stordalen between 4.1 and 1.9 ka. In contrast, non-overlapping confidence intervals indicate significantly different SHD ages of 9.1–7.7 ka and 5.1–3.7 ka for Vanndalen 2 and Vanndalen 1, respectively.

R-value frequency distributions

The frequency distributions of *R*-values from the talus slopes (Figure 8) differ in shape from those of the control points (Figure 6). The asymmetrical distributions of the talus slopes are characterised by various degrees of negative skew with relatively long lower tails. In contrast, the control surfaces have near symmetrical distributions without long lower tails. The kurtosis of the talus-slope distributions tend to be intermediate in comparison to the strongly peaked (leptokurtic) distribution of the young control surface and the broader, platykurtic distribution of the old control surface. Two of the distributions, Vetlestølsdalen 1 and Vanndalen 2, exhibit evidence of secondary modes below the mean value of the old control surface (*R*-values of 30–33), but these modes are poorly developed. Such differences in skew, kurtosis and modality of the talus-slope distributions are interpretable in relation to the diachronous nature of talus-slope surfaces (see below).
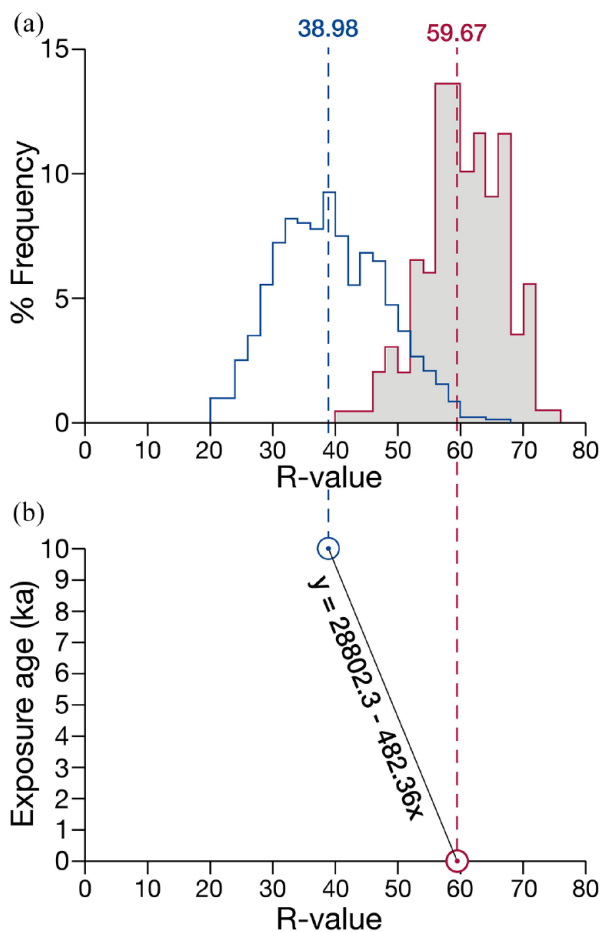
Discussion

SHD ages from talus slopes as diachronous surfaces

SHD ages derived from boulder landforms represent the average exposure-age of a large number of boulders, that is the average time elapsed since exposure of the boulder surfaces to subaerial weathering (see Matthews and Winkler, 2022; Matthews et al., 2014). The meaning of a SHD age is simple for a landform, such as a recessional moraine or rock-slope failure, deposited by a single event over a very short time span (at one moment in time or perhaps over decades or even centuries). Such synchronous surfaces are characterised by boulders all of which were exposed to

Table 2. *R*-values from three levels on eight talus slopes (*n* = 200 impacts for each level at each site). Sites are located on Figure 1.

Talus site	Lower level			Mid level			Upper level			All levels combined		
	Mean	SD	CI	Mean	SD	CI	Mean	SD	CI	Mean	SD	CI
Site 1 (Sprongdalen)	50.16	9.87	1.37	51.03	9.18	1.27	51.52	8.32	1.15	50.90	9.12	0.73
Site 2 (Sprongdalen)	48.79	9.32	1.29	52.84	9.03	1.25	51.75	8.68	1.20	51.13	8.99	0.72
Site 3 (Stordalen)	54.96	10.59	1.47	53.63	9.92	1.38	54.27	9.56	1.33	54.28	10.02	0.80
Site 4 (Stordalen)	53.57	9.10	1.26	51.86	10.14	1.41	52.50	8.72	1.21	52.65	9.34	0.75
Site 5 (Vetlestølsdalen)	46.19	10.80	1.50	45.97	10.66	1.48	47.25	11.67	1.62	46.47	11.04	0.88
Site 6 (Vetlestølsdalen)	48.74	9.28	1.29	47.61	9.17	1.27	48.18	8.85	1.23	48.18	9.09	0.73
Site 7 (Vanndalen)	50.88	8.70	1.21	50.51	8.51	1.18	50.25	9.26	1.28	50.54	8.82	0.71
Site 8 (Vanndalen	42.38	9.08	1.23	44.36	9.94	1.38	40.02	9.20	1.28	42.25	9.40	0.75

SD: standard deviation; CI: 95% confidence interval.

Figure 6. (a) *R*-value distributions and mean *R*-values of the old (blue) and new (red and shaded) control points linked to (b) the linear relationship between mean *R*-value and surface age and the age-calibration equation.

are Mid- to Late-Holocene, ranging from 6390 ± 775 years (Vetlestølsdalen 1) to 2620 ± 740 years (Stordalen 1). Combined with evidence from the *R*-value distributions, these *average* exposure ages of the surface boulders indicate that the talus slopes are essentially relict, diachronous surfaces with low levels of modern activity. This conclusion is supported by the small number of boulders that lack lichen growth as well as the frequency distributions of *R*-values (Figure 8). Even in the case of the youngest SHD age (Stordalen 1), the mean *R*-value is >5 units lower than that of the (synchronous) modern control surface. Furthermore, *R*-values as low as 20–40, which are characteristic of the (synchronous) old control surface (Figure 6) are present in appreciable numbers on the talus slopes.

The negative skew of the talus slope *R*-value distributions appear, moreover, to be a reliable indicator of the presence of surface boulders with a relatively old exposure age. The boulders that comprise the ends of the lower tails of the distributions likely survived burial by later talus deposition. This interpretation is consistent with the association of the youngest SHD ages (Stordalen 1 and 2) with the longest, tapering lower tails, which contain only a small number of boulders with low *R*-values. The four relatively old talus slopes from Vanndalen and Vetlestølsdalen exhibit more platykurtic distributions with a higher frequency of boulders characterised by low *R*-values and/or a tendency in some cases towards secondary modes close to the mean *R*-value of the old control-point distribution. The near-symmetrical distribution of the *R*-values from the oldest talus slope (Vanndalen 2) provides the exception that proves the rule. This talus slope is close to the (synchronous) old control surface in terms of both its *R*-value distribution and SHD age. Its combination of a high frequency of *R*-values <40 with an equally anomalously low frequency of *R*-values > 60 indicates a relict landform with an almost complete lack of modern activity.

### Talus slope development, rockfall activity and environmental change

Prior to regional deglaciation around 10,000 years ago, it can be assumed that during successive glaciations, scouring by ice streams efficiently eroded oversteepened valley sides even though plateau landscapes may have been little affected by cold-based ice sheets (Andersen et al., 2018, 2019; Kleman et al., 2008; Nesje and Willans, 1994). During and following deglaciation, rock-slope instability would have been high as a consequence of such factors as ice-sheet thinning, glacial debutressing, glacio-isostatic uplift and seismic shock (Böhme et al., 2015; Curry, 2021; Hermanns et al., 2017). Paraglacial triggering is likely to have led to higher rates of rock-slope failure and rockfall and hence faster development of talus-slopes than later in the Holocene (Blikra and Nemec, 1998; Matthews and Nesje, 2022; Rapp, 1960).

the atmosphere at approximately the same time. The interpretation is more complex for diachronous surfaces, such as talus slopes, alluvial fans, rock glaciers and protalus ramparts, which consist of boulders that were deposited continuously or incrementally over millennia. Thus, whereas the SHD age of a synchronous surface may approximate the landform age, that is the time elapsed since the onset of the formation of the landform, the exposure age of a diachronous surface provides only a minimum estimate of landform age, which may be appreciably younger than the landform age.

With the exception of one site (Vanndalen 2, 8425 ± 700 years), Figure 7 demonstrates that the SHD ages from the talus slopes

Table 3. *R*-values and SHD ages from the eight talus slopes (600 impacts per talus; data from all levels combined).

Talus site	R-values			Exposure ages and errors (year)		
	Mean	SD	CI	SHD age (±95% CI)	Sampling error (Cs)	Calibration error (Cc)
Site 1 (Sprongdalen)	50.90	9.12	0.73	4250 ± 700	500	495
Site 2 (Sprongdalen)	51.13	8.99	0.72	4140 ± 695	490	490
Site 3 (Stordalen)	54.28	10.02	0.80	2620 ± 740	550	500
Site 4 (Stordalen)	52.65	9.34	0.75	3405 ± 710	510	495
Site 5 (Vetlestølsdalen)	46.47	11.04	0.88	6390 ± 775	605	485
Site 6 (Vetlestølsdalen)	48.18	9.09	0.73	5560 ± 695	495	485
Site 7 (Vanndalen)	50.54	8.82	0.71	4425 ± 690	480	490
Site 8 (Vanndalen)	42.25	9.40	0.75	8425 ± 700	515	475

SD: standard deviation; CI: 95% confidence interval.
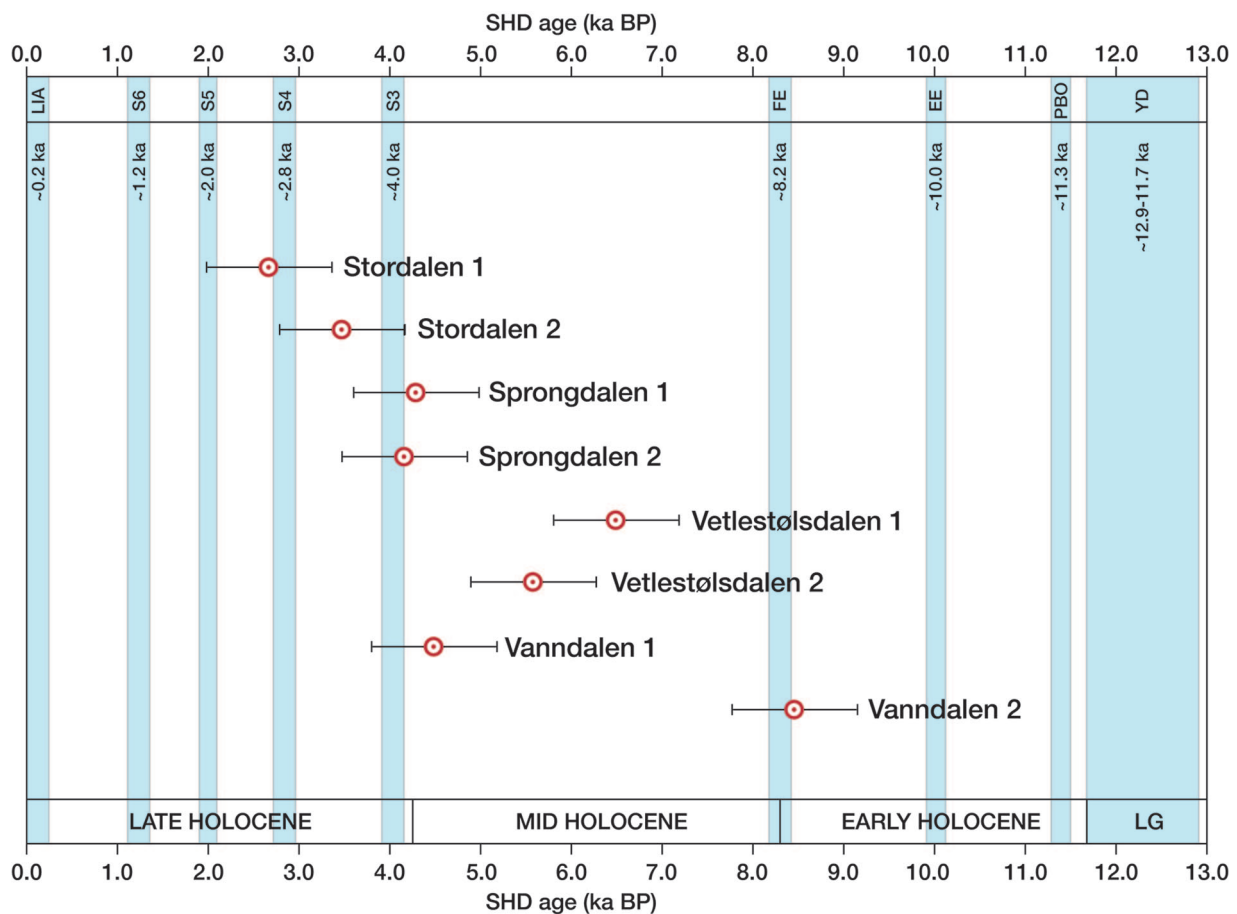
Figure 7. SHD ages (with 95% confidence intervals) of eight talus slopes in relation to the maxima of centennial- to millennial-scale glacier-expansion episodes indicative of cold periods in southern Norway (cf. Bakke et al., 2010; Nesje and Matthews, 2024; Matthews and Dresser, 2008).
YD: Younger Dryas; PBO: Preboreal Oscillation; EE: Erdalen Event; FE: Finse Event; S3: Smørstabbtindan Event III; S4: Smørstabbtindan Event IV; S5: Smørstabbtindan Event V; S6: Smørstabbtindan Event VI; LIA: Little Ice Age.

Secondary modes in our talus-slope *R*-value distributions (Figure 8), which lie close to the mean *R*-value of the older control surface, are consistent with this concept of a paraglacial maximum in the accumulation of talus.

Later in the Holocene, as the paraglacial influence waned, rapid warming (Eldevik et al., 2014; Mauri, et al., 2015) would have provided a new source of rock-slope instability, namely permafrost degradation. Evidence of significant slope instability from this source is widespread in southern Norway in relation to rock-slope failures both large (Hilger et al., 2018, 2021) and small (Matthews et al., 2018). The small rock-slope failures in Jotunheimen ranging in volume from 12 to 2520 m² increased in frequency during the Early- and Mid-Holocene reaching peak frequency at ~4.5 ka, close to the end of the Holocene Thermal Maximum when permafrost depth was at a minimum (Matthews et al., 2018). The decline in activity after that date was attributed to the exhaustion of permafrost at depths shallow enough to host small rock-slope failures. Rates of rockfall activity, defined as the release of individual rock particles from rock-slopes, are likely to have had a similar response to thawing permafrost, and hence to have contributed to the continued growth of talus-slopes as well as related landforms such as pronival (protalus) ramparts (Matthews and Wilson, 2015; Matthews et al., 2011) and snow-avalanche fans (Matthews et al., 2020). However, peak rockfall
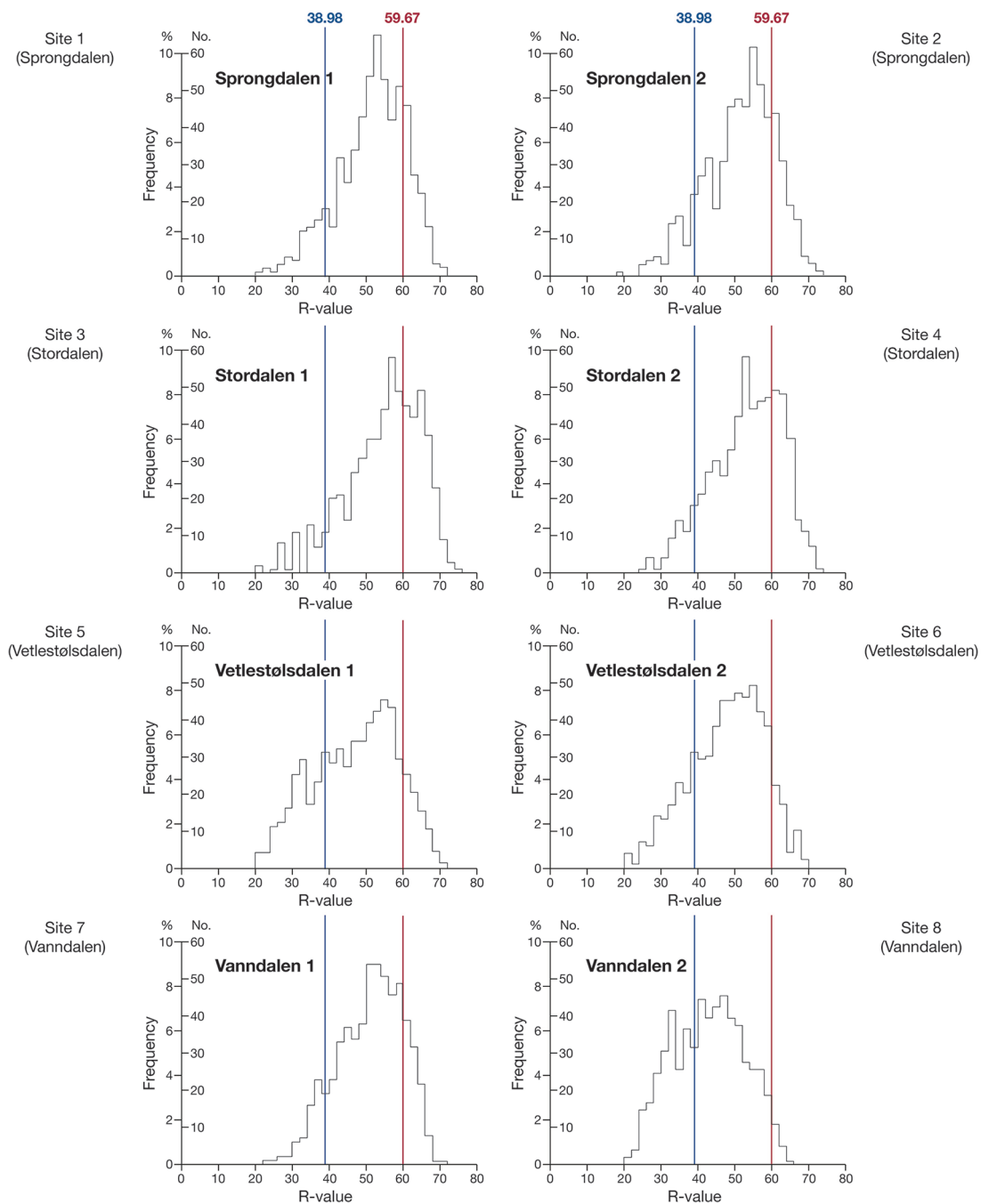
Figure 8. *R*-value distributions for eight talus slopes. Each frequency histogram is based on 600 *R*-values. Vertical lines indicate the mean *R*-values for old (left, blue) and young (right, red) control points.

activity associated with permafrost degradation may have occurred earlier in the Jostedalen area because the rock faces there occur further below the lower altitudinal limit of mountain permafrost than in Jotunheimen (cf. Etzelmüller et al., 2003; Lilleøren et al., 2012; Magnin et al., 2019; Matthews and Nesje, 2022).

Different climatic controls on talus-slope development seem to have come into play in the Late-Holocene, when seasonal frost rather than permafrost affected rockfall activity. Blikra and Nesje (1997) and Blikra and Nemec (1998) record a progressive increase in rockfall activity after ~3.8 ka interrupted by the development of radiocarbon-dated humic palaeosols, which signify stable phases with non-deposition of talus. Cooler and possibly wetter conditions appear to be associated with the increase in active talus deposition in the Late-Holocene and also with shorter-lived

episodes of activity dated by lichenometry and analysed further by simulation modelling (McCarroll et al., 1998, 2001). They concluded that the rate of rockfall-talus accumulation in the 18th century (the coldest phase of the Little Ice Age) could have been five times the background rate during the Late-Holocene. Similar episodes of enhanced activity might be postulated for several other centennial- to millennial-scale glacier-expansion episodes, which are indicative of intervals of relatively cold climate (see Figure 7). However, the SHD evidence from the present study indicates that most talus-slope development took place as a result of paraglacial rockfall in the Early Holocene followed by generally low acquisition of debris thereafter. Little rockfall activity occurred at our sites during the Little Ice Age (unless it was deposited on the upper slopes and did not affect the mid and lower slopes).

Differences in SHD ages between sites indicate that local factors moderate regional controls on rates of rockfall and talus accumulation. In general, talus slopes in Stordalen and Sprongdalen at altitudes of 500–700 m a.s.l. yielded younger exposure ages than those around 1000 m a.s.l. in Vetlestølsdalen and Vanndalen. For three of the valleys (Stordalen, Sprongdalen and Vetlestølsdalen), overlapping confidence intervals indicate site pairs that do not differ significantly in exposure age. Local geological differences and/or differences in the extent of the bedrock cliffs between valleys likely provide such valley-specific controls, which would bear further investigation. The anomalous *R*-value distribution and exposure age of the Vanndalen 2 site may have been affected by one or more rock-slope failures in the Early Holocene, the debris from which survived later burial.

The chance of survival of highly weathered surface boulders with relatively old exposure ages, especially at the distal fringe of talus slopes, increases if the rate of accumulation of talus is slow. Under such circumstances, it is possible but unlikely that the SHD age of such diachronous surfaces may approximate the onset of talus-slope formation (landform age). On more active talus accumulations with higher rates of rockfall, the younger exposure-age of surface boulders should be more useful as an indicator of the extent of modern activity, with exceptionally active landforms yielding modern ages.

Conclusions

We demonstrate, for the first time, the detailed application of SHD to talus-slopes with implications for other coarse-grained depositional landforms with diachronous surfaces (such as rock glaciers, pronival ramparts, snow-avalanche landforms and alluvial fans). Our SHD dates, which range from late in the Early Holocene to early in the Late-Holocene, represent the average exposure age of the surface boulders, and reflect spatial and temporal variation in the rate of rockfall activity. With the aid of an analysis of *R*-values distributions, relatively old SHD ages are interpreted as indicating the primary importance of Early Holocene paraglacial instability of oversteepened rock slopes following regional deglaciation, combined with later permafrost degradation associated with the Holocene Thermal Maximum and short-term Late-Holocene cold-climate events. Generally slow rates of talus accumulation led to inefficient burial of surface material, especially on the distal part of the talus slope, and survival at the talus-slope surface of boulders with a relatively old exposure-age. However, SHD ages from talus slopes and other diachronous surfaces, provide only minimum estimates of landform age (defined as the timing of the onset of landform formation). Even where deposition rates are low, SHD ages are unlikely to be close estimates of landform age. On the other hand, SHD ages can be a reliable estimate of land-surface age and, where deposition rates are relatively high SHD ages should prove useful for inferring land-surface dynamics and as an indicator of modern activity levels.

Author contributions

John A Matthews: Conceptualization; Formal analysis; Investigation; Methodology; Writing – original draft; Writing – review & editing.
Richard W. Mourne: Investigation; Writing – review & editing.

ORCID iD

John A Matthews https://orcid.org/0000-0002-2610-863X

References

Andersen JL, Egholm DL, Knudsen MF et al. (2018) Widespread erosion on high plateaus during recent glaciations in Scandinavia. *Nature Communications* 9: 830. DOI: 10.1028/$41467-018-03280-2.

Andersen JL, Egholm DL, Knudsen MF et al. (2019) Pleistocene evolution of a Scandinavian plateau landscape. *Journal of Geophysical Research Earth Surface* 123: 3370–3387.

André M-F (1997) Holocene rockwall retreat in Svalbard: a triple-rate evolution. *Earth Surface Processes and Landforms* 22: 423–440.

Aune B (1993) Temperatur Normaler, Normalperiode 1961-1990. Rapport 02/93, Den Norske Meteorologiske Institutt, Oslo.

Bakke J, Dahl SO, Paasche Ø et al. (2010) A complete record of Holocene glacier variability at Austre Okstindbreen, northern Norway: An integrated approach. *Quaternary Science Reviews* 29: 1246–1262.

Ballantyne CK (2018) *Periglacial Geomorphology*. Chichester: Wiley.

Bickerton RW and Matthews JA (1992) On the accuracy of lichenometric dates: An assessment based on the 'Little Ice Age' moraine sequence of Nigardsbreen, southern Norway. *The Holocene* 2: 227–237.

Bickerton RW and Matthews JA (1993) 'Little Ice Age' variations of outlet glaciers from the Jostedalsbreen ice cap, southern Norway: A regional lichenometric-dating study of ice-marginal moraine sequences and their climatic significance'. *Journal of Quaternary Science* 8: 45–66.

Blikra JH and Nemec W (1998) Postglacial colluvium in western Norway: Depositional processes, facies and palaeoclimatic record. *Sedimentology* 45: 909–959.

Blikra LH and Nesje A (1997) Holocene avalanche activity in western Norway: Chronostratigraphy and palaeoclimatic implications. In: Matthews JA, Brunsden D, Frenzel B et al. (eds) *Rapid Mass Movement as a Source of Climatic Evidence for the Holocene*. Stuttgart: Gustav Fischer Verlag, pp.299–312.

Böhme M, Oppikofer T, Longva O et al. (2015) Analyses of past and present rock slope instabilities in a fjord valley: Implications for hazard estimations. *Geomorphology* 248: 464–474.

Chinn TJH (1981) Use of rock weathering-rind thickness for Holocene absolute age-dating in New Zealand. *Arctic and Alpine Research* 13: 33–45.

Colman SM and Dethier DP (eds) (1986) *Rates of Chemical Weathering of Rocks and Minerals*. Orlando, FL: Academic Press.

Curry AM (2021) Paraglacial rock-slope failure following deglaciation in Western Norway. In: Beylich AA (ed.) *Landscapes and Landforms of Norway*. Cham: Springer Nature, pp.97–130.

Curry AM and Black R (2003) Structure, sedimentology and evolution of rockfall talus, Mynydd Ddu, south Wales. *Proceedings of the Geologists' Association* 114: 49–64.

Dahl SO, Nesje A, Lie Ø et al. (2002) Timing, equilibrium-line altitudes and climatic implications of two early Holocene glacier readvances during the Erdalen Event at Jostedalsbreen, western Norway. *The Holocene* 12: 17–25.

Eldevik T, Risebrobakken B, Bjune A et al. (2014) A brief history of climate – the northern seas from the Last Glacial

Maximum to global warming. *Quaternary Science Reviews* 106: 225–246.

Etzelmüller B, Berthling I and Sollid JL (2003) Aspects and concepts on the geomorphological significance of Holocene permafrost in southern Norway. *Geomorphology* 52: 87–104.

Førland EJ (1993) Nedbørnormaler, Normalperiode 1961-1990. Rapport 39/93, Den Norske Meteorologiske Institutt, Oslo.

Francou B and Manté C (1990) Analysis of the segmentation in the profile of alpine talus slopes. *Permafrost and Periglacial Processes* 1: 53–60.

Gjerde M, Hoel O and Nesje A (2023) The 'Little Ice Age' advance of Nigardsbreen, Norway – a cross disciplinary revision of the chronological framework. *The Holocene* 33: 1362–1375.

Grove JM (1988) *The Little Ice Age*. London: Methuen.

Hermanns RL, Schleier M, Böhme M et al. (2017) Rock avalanche activity in W and S Norway peaks after the retreat of the Scandinavian ice sheet. In: Mikos M, Vilímek V, Yin Y et al. (eds) *Advancing Culture of Living with Landslides, Volume 5: Landslides in Different Environments*. Heidelberg: Springer, pp.331–338.

Hétu B and Gray JT (2000) Effects of environmental change on scree slope development throughout the postglacial period in the Chic-Choc Mountains in the northern Gaspé Peninsula, Québec. *Geomorphology* 32: 135–155.

Hilger P, Hermanns RL, Czekirda J et al. (2021) Permafrost as a first order control on long-term rock-slope deformation in (Sub-)Arctic Norway. *Quaternary Science Reviews* 251: 106718.

Hilger P, Hermanns RL, Gosse JC et al. (2018) Multiple rock-slope failures from Mannen in Romsdal Valley, western Norway, revealed from Quaternary geological mapping and [10]Be exposure dating. *The Holocene* 28: 1841–1854.

Hinchliffe S (1999) Timing and significance of talus slope reworking, Trotternish, Skye, northwest Scotland. *The Holocene* 9: 483–494.

Hinchliffe S and Ballantyne CK (2009) Talus structure and evolution on sandstone mountains in Scotland. *The Holocene* 19: 477–486.

Hughes ALC, Gyllencreutz R, Lohne Ø et al. (2016) The last Eurasian ice sheets – a chronological database and time-slice reconstruction, DATED-1. *Boreas* 45: 1–45.

Innes JL (1983) Stratigraphic evidence of episodic talus accumulation on the Isle of Skye, Scotland. *Earth Surface Processes and Landforms* 8: 399–403.

Karakul H (2017) Investigation of saturation effect on the relationship between compressive strength and Schmidt hammer rebound. *Bulletin of Engineering Geology and the Environment* 76: 1143–1152.

Karakul H (2020) Investigation of the effect of impact direction on Schmidt rebound values by multivariate regression and neuro-fuzzy models. *Springer Nature Applied Sciences* 2: 1807.

Kleman J, Stroeven AP and Lundqvist J (2008) Patterns of Quaternary ice sheet erosion and deposition in Fennoscandia and a theoretical framework for explanation. *Geomorphology* 97: 73–90.

Lafortune M, Filion L and Hétu B (1997) Dynamique d'un front forestier sur un talus d'éboulis actif en climat tempéré froid (Gaspésie, Québec). *Géographie Physique et Quaternaire* 51: 1–15.

Lilleøren KS, Etzelmüller B, Schuler TV et al. (2012) The relative age of mountain permafrost — estimation of Holocene permafrost limits in Norway. *Global and Planetary Change* 92–93: 209–223.

Luckman BH (2013) Talus slopes. In: Elias SA and Mock CJ (eds) *Encyclopedia of Quaternary Science, Volume 3*. Amsterdam: Elsevier, pp.566–573.

Lutro O and Tveten E (1996) *Geologiske kart over Norge, Berggrunnskart Årdal, Målestokk 1:250,000*. Trondheim: Norges Geologiske Undersøkelse.

Magnin F, Etzelmüller B, Westermann S et al. (2019) Permafrost distribution in steep rock slopes in Norway: Measurements, statistical modelling and implications for geomorphic processes. *Earth Surface Dynamics* 7: 1019–1040.

Mangerud J, Hughes ALC, Johnson MD et al. (2023) The Fennoscandian Ice Sheet during the Younger Dryas stadial. In: Palacios D, Hughes PD, García-Ruiz JM and Andrés N (eds) *European Glacial Landscapes. The Last Deglaciation*. Amsterdam: Elsevier, pp.437–452.

Matthews JA (1981) *Quantitative and Statistical Approaches to Geography: A Practical Manual*. Oxford: Pergamon Press.

Matthews JA and Dresser PQ (2008) Holocene glacier variation chronology of the Smørstabbtindan massif, Jotunheimen, Norway, and the recognition of European Neoglacial Events. *The Holocene* 18: 181–201.

Matthews JA, Haselberger S, Hill J et al. (2020) Snow-avalanche boulder fans in Jotunheimen, southern Norway: Schmidt-hammer exposure-age dating, geomorphometrics, dynamics and evolution. *Geografiska Annaler Series A (Physical Geography)* 102: 118–140.

Matthews JA, Linge H, Nesje A et al. (2023) Deglaciation of the highest mountains in Scandinavia at the Younger Dryas-Holocene transition: Evidence from surface exposure-age dating of ice-marginal moraines. *Boreas* 53: 139–163.

Matthews JA and McEwen L (2013) High-precision Schmidt-hammer exposure-age dating (SHD) of flood berms, Vetlestølsdalen, alpine southern Norway: First application and some methodological issues. *Geografiska Annaler Series A (Physical Geography)* 95: 185–195.

Matthews JA, McEwen L and Owen G (2015) Schmidt-hammer exposure-age dating (SHD) of snow-avalanche impact ramparts in southern Norway: Approaches, results and implications for landform age, dynamics and development. *Earth Surface Processes and Landforms* 40: 1705–1718.

Matthews JA, Mourne RW, Wilson P et al. (2024) Schmidt-hammer R-values from glacially-scoured bedrock surfaces across glacier-foreland boundaries: Insights into Holocene weathering rates with implications for exposure-age dating. *Geomorphology* 454: 109139.

Matthews JA and Nesje A (2022) Scandinavia. In: Oliva M, Nývlt D and Fernández-Fernández JM (eds) *Periglacial Landscapes of Europe*. Cham: Springer, pp.365–426.

Matthews JA and Owen G (2010) Schmidt hammer exposure-age dating: Developing linear age-calibration curves using Holocene bedrock surfaces from the Jotunheimen-Jostedalsbreen regions of southern Norway. *Boreas* 39: 105–115.

Matthews JA, Owen G, Winkler S et al. (2016) A rock-surface microweathering index from Schmidt hammer R-values and its preliminary application to some common rock types in southern Norway. *Catena* 143: 35–44.

Matthews JA, Shakesby RA, Owen G et al. (2011) Pronival rampart formation in relation to snow-avalanche activity and Schmidt-hammer exposure-age dating (SHD): Three case studies from southern Norway. *Geomorphology* 130: 280–288.

Matthews JA, Shakesby RA, Schnabel C et al. (2008) Cosmogenic [10]Be and [26]Al ages of Holocene moraines in southern Norway I: Testing the method and confirmation of the date of the Erdalen Event (c.10 ka) at its type site. *The Holocene* 18: 1155–1164.

Matthews JA and Wilson P (2015) Improved Schmidt-hammer exposure ages for active and relict pronival ramparts in southern Norway and their palaeoenvironmental implications. *Geomorphology* 246: 7–21.

Matthews JA and Winkler S (2011) Schmidt hammer exposure-age dating (SHD): Application to early Holocene moraines and a reappraisal of the reliability of cosmogenic-nuclide dating (TCND) at Austanbotnbreen, Jotunheimen, Norway. *Boreas* 40: 256–270.

Matthews JA and Winkler S (2022) Schmidt-hammer exposure-age dating: A review of principles and practice. *Earth-Science Reviews* 230: 104038.

Matthews JA, Winkler S and Wilson P (2014) Age and origin of ice-cored moraines in Jotunheimen and Breheimen, Southern Norway: Insights from Schmidt-hammer exposure-age dating. *Geografiska Annaler Series Series A (Physical Geography)* 96: 531–548.

Matthews JA, Winkler S, Wilson P et al. (2018) Small rock-slope failures conditioned by Holocene permafrost degradation: A new approach and conceptual model based on Schmidt-hammer exposure-age dating, Jotunheimen, southern Norway. *Boreas* 47: 1144–1169.

Mauri A, Davis BAS, Collins PM and Kaplan JO (2015) The climate of Europe during the Holocene: A gridded pollen-based reconstruction and its multi-proxy evaluation. *Quaternary Science Reviews* 112: 109–127.

McCarroll D (1994) A new approach to lichenometry: Dating single-age and diachronous surfaces. *The Holocene* 4: 393–396.

McCarroll D, Shakesby RA and Matthews JA (1998) Spatial and temporal patterns of late-Holocene rockfall activity on a Norwegian talus slope: A lichenometric and simulation modelling approach. *Arctic and Alpine Research* 30: 51–60.

McCarroll D, Shakesby RA and Matthews JA (2001) Enhanced rockfall activity during the Little Ice Age: Further lichenometric evidence from Norwegian talus. *Permafrost and Periglacial Processes* 12: 157–164.

Mottershead DN and Colin RL (1976) A study of Flandrian glacier fluctuations in Tunsbergdalen, southern Norway. *Norsk Geologisk Tidsskrift* 56: 413–436.

Moya J, Corominas J, Pérez Arcas J and Baeza C (2010) Tree-ring based assessment of rockfall frequency on talus slopes at Solàd'Andorra, Eastern Pyrenees. *Geomorphology* 118: 393–408.

Nesje A (2009) Latest Pleistocene and Holocene alpine glacier fluctuations in Scandinavia. *Quaternary Science Reviews* 28: 2119–2136.

Nesje A, Kvamme M, Rye N et al. (1991) Holocene glacial and climate history of the Jostedalsbreen region, western Norway; evidence from lake sediments and terrestrial deposits. *Quaternary Science Reviews* 10: 87–114.

Nesje A and Matthews JA (2024) Holocene glacial landscapes of the Scandinavian Peninsula. In: Palacios D, Hughes PD, Jomelli V and Tanarro LM (eds) *European Glacial Landscapes: The Holocene*. Chennai: Elsevier, pp.245–274.

Nesje A, Matthews JA, Linge H et al. (2021) New evidence for active talus-foot rock glaciers at Øyberget, southern Norway, and their development during the Holocene. *The Holocene* 31: 1786–1796.

Nesje A and Willans IM (1994) Erosion of Sognefjord, Norway. *Geomorphology* 9: 33–45.

Østrem G, Liestøl O and Wold B (1977) Glaciological investigations at Nigardsbreen, Norway. *Norsk Geografisk Tidsskrift* 30: 187–209.

Peña-Monné JL, Sampietro-Vattuone MM, Picazo-Millán J et al. (2024) Block alignments/talus flatiron stages as response to lithological factors and dynamic slope changes in the Central Ebro Basin, NE Spain. *Quaternary Science Reviews* 340: 108864.

Perret S, Stoffel M and Kienholz H (2006) Spatial and temporal rockfall activity in a forest stand in the Swiss Prealps – A dendrogeomorphological case study. *Geomorphology* 74: 219–231.

Proceq SA (2017) *Concrete Test Hammer 'Original Schmidt' Operating Instructions*. Schwerzenbach: Proceq SA.

Rapp A (1960) Recent development of mountain slopes in Kärkevagge and surroundings, northern Scandinavia. *Geografiska Annaler* 42: 65–200.

Rixhon G and Desmoulin A (2013) Evolution of slopes in a cold climate. In: Shroder J, Giardino R and Harbor J (eds) *Treatise on Geomorphology, Volume 8 (Glacial and Periglacial Geomorphology)*. San Diego, CA: Academic Press, pp.393–415.

Sanders D (2010) Sedimentary facies and progradational style of a Pleistocene talus slope succession, northern calcareous Alps, Austria. *Sedimentary Geology* 228: 271–283.

Santos-González J, González-Gutiérrez RB, Gómez-Villar A et al. (2024) Application of the Schmidt-hammer for relative-age dating of glacial and periglacial landforms in the Cantabrian Mountains (NW Spain). *Geomorphology* 456: 109210.

Sass O (2010) Spatial and temporal pattern of rockfall activity – a lichenometric approach in the Stubaier Alps, Austria. *Geografiska Annaler Series A (Physical Geography)* 92: 375–391.

Scapozza C, Del Siro C, Lambiel C and Ambrosi1 C (2021) Schmidt hammer exposure-age dating of periglacial and glacial landforms in the Southern Swiss Alps based on *R*-value calibration using historical data. *Geografica Helvetica* 76: 401–423.

Scotti R, Brardinoni F, Crosta G et al. (2017) Time constraints for post- LGM landscape response to deglaciation in Val Viola, Central Italian Alps. *Quaternary Science Reviews* 177: 10–33.

Shakesby RA, Matthews JA, Karlén W and Los SO (2011) The Schmidt hammer as a Holocene calibrated-age dating technique: Testing the form of the R-value-age relationship and defining the predicted-age errors. *The Holocene* 21: 615–628.

Shakesby RA, Matthews JA and Owen G (2006) The Schmidt hammer as a relative-age dating tool and its potential for calibrated-age dating in Holocene glacial environments. *Quaternary Science Reviews* 25: 2846–2867.

Shepherd B, Portenga EW and Peplinski AJ (2024) Quantifying the effects of carborundum rock surface smoothing for Schmidt hammer R-value metrics measured on glacial erratics in the North American Great Lakes region. *Earth Surface Processes and Landforms* 49: 4077–4987.

Siegel S (1956) *Nonparametric Statistics for the Behavioral Sciences*. New York, NY: McGraw-Hill.

Šilhán K (2010) Dendrogeomorphology of spatiotemporal activity of rockfall in the Flysch Carpathians: A case study on the western slope of Mt. Smrk (Moravskoslezské Beskydy Mts, Czech Republic). *Moravian Geographical Reports* 18: 33–42.

Stahl T, Winkler S, Quigley M et al. (2013) Schmidt hammer exposure-age dating (SHD) of late Quaternary fluvial terraces in New Zealand. *Earth Surface Processes and Landforms* 38: 1838–1850.

Statham I (1976) A scree slope rockfall model. *Earth Surface Processes* 1: 43–62.

Stoffel M, Bollschweiler M and Hasler G (2006) Differentiating past events on a cone influenced by debris-flow and snow avalanche activity — a dendrogeomorphological approach. *Earth Surface Processes and Landforms* 31: 1424–1437.

Stoffel M, Lièvre I, Conus D et al. (2005b) 400 years of debris-flow activity and triggering weather conditions: Ritigraben, Valais, Switzerland. *Arctic, Antarctic, and Alpine Research* 37: 387–395.

Stoffel M, Lievre I, Monbaron M and Perret S (2005a) Seasonal timing of rockfall activity on a forested slope at Taschgüfer (Valais, Swiss Alps) — a dendrochronological approach. *Zeitschrift für Geomorphologie* 49: 89–106.

Sumner P and Nel W (2002) The effect of rock moisture on Schmidt hammer rebound: Tests on rock samples from Marion Island and South Africa. *Earth Surface Processes and Landforms* 27: 1137–1142.

Sumner P, Nel W, Holness S and Boelhouwers C (2002) Rock weathering characteristics as relative-age indicators for glacial and post-glacial landforms on Marion Island. *South African Geographical Journal* 84: 153–157.

Tomkins MD, Dortch JM and Hughes PD (2016) Schmidt hammer exposure dating (SHED), establishment and implications for the retreat of the last British Ice Sheet. *Quaternary Geochronology* 33: 46–60.

Tomkins MD, Dortch JM, Hughes PD et al. (2018b) Schmidt hammer exposure dating (SHED): Rapid age assessment of glacial landforms in the Pyrenees. *Quaternary Research* 90: 26–37.

Tomkins MD, Hucka JJ, Dortch JM et al. (2018a) Schmidt hammer exposure dating (SHED): Calibration procedures, new exposure age data and an online calculator. *Quaternary Geochronology* 44: 55–62.

Trenbirth HE and Matthews JA (2010) Lichen growth rates on glacier forelands in southern Norway: Preliminary results from a 25-year monitoring programme. *Geografiska Annaler, Series A (Physical Geography)* 92: 19–39.

Whitehouse IE and McSaveney MJ (1983) Diachronous talus surfaces in the Southern Alps, New Zealand, and their implications to talus accumulation. *Arctic and Alpine Research* 15: 53–64.

Whitehouse IE, McSaveney MJ and Chinn TJ (1980) Dating your scree. *Review of the Tussock Grassland and Mountainlands Institute* 39: 15–25.